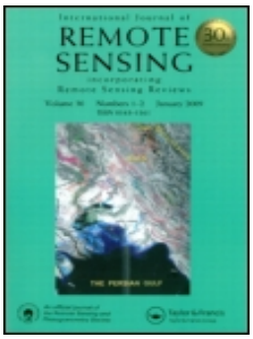

International Journal of Remote Sensing

ISSN: 0143-1161 (Print) 1366-5901 (Online) Journal homepage: www.tandfonline.com/journals/tres20

Object-based change detection using correlation image analysis and image segmentation

J. Im, J. R. Jensen & J. A. Tullis

To cite this article: J. Im, J. R. Jensen & J. A. Tullis (2008) Object-based change detection using correlation image analysis and image segmentation, International Journal of Remote Sensing, 29:2, 399-423, DOI: 10.1080/01431160601075582

To link to this article: https://doi.org/10.1080/01431160601075582

International Journal of Remote Sensing
Vol. 29, No. 2, 20 January 2008, 399–423

Taylor & Francis
Taylor & Francis Group

Object-based change detection using correlation image analysis and image segmentation

J. IM*†, J. R. JENSEN† and J. A. TULLIS‡

†Center for GIS and Remote Sensing, Department of Geography, University of South Carolina, Columbia, SC 29208, USA

‡Department of Geosciences, University of Arkansas, Fayetteville, AR 72701, USA

(*Received 24 May 2006; in final form 20 November 2006*)

This study introduces change detection based on *object/neighbourhood correlation image* analysis and image segmentation techniques. The correlation image analysis is based on the fact that pairs of brightness values from the same geographic area (e.g. an object) between bi-temporal image datasets tend to be highly correlated when little change occurres, and uncorrelated when change occurs. Five different change detection methods were investigated to determine how new contextual features could improve change classification results, and if an object-based approach could improve change classification when compared with per-pixel analysis. The five methods examined include (1) object-based change classification incorporating *object correlation images* (OCIs), (2) object-based change classification incorporating *neighbourhood correlation images* (NCIs), (3) object-based change classification without contextual features, (4) per-pixel change classification incorporating NCIs, and (5) traditional per-pixel change classification using only bi-temporal image data. Two different classification algorithms (i.e. a machine-learning decision tree and nearest-neighbour) were also investigated. Comparison between the OCI and the NCI variables was evaluated. Object-based change classifications incorporating the OCIs or the NCIs produced more accurate change detection classes (Kappa approximated 90%) than other change detection results (Kappa ranged from 80 to 85%).

1. Introduction

The proliferation of high-spatial resolution multispectral imagery from satellite and aerial sensors (e.g. IKONOS from GeoEye, Inc., QuickBird from DigitalGlobe, Inc., ADS40 from Leica Geosystems, Inc.) has significantly changed the level of sophistication required in digital image processing. In particular, many traditional image processing techniques based on per-pixel analysis may not function successfully with high-spatial resolution imagery due to high-frequency components and horizontal layover caused by off-nadir look angles. To overcome this problem, several new algorithms include contextual information (e.g. neighbourhood correlation images) and pixel region properties such as shape (Walter 2004, Im and Jensen 2005, Syed *et al.* 2005).

Object-based image analysis based on multi-resolution image segmentation techniques has demonstrated significant advantages for analysing high-spatial

*Corresponding author. Email: ersgis@gmail.com

International Journal of Remote Sensing
ISSN 0143-1161 print/ISSN 1366-5901 online
http://www.tandf.co.uk/journals
DOI: 10.1080/01431160601075582

resolution imagery. Object-based analysis subdivides the image into meaningful homogeneous regions based not only on spectral properties but also on shape, texture, size, and other topological features, and organizes them hierarchically as image objects (also referred to as image segments) (Benz *et al.* 2004, Blaschke 2005). The segmentation procedure (extraction of the image objects) is controlled by the user-specified scale (size) or resolution of the expected objects (deKok *et al.* 1999). Object-based approaches have been successful for land-use and land-cover classification (e.g. Laliberte *et al.* 2004, Frohn *et al.* 2005, Jensen *et al.* 2006).

There is great interest in change detection using high-spatial resolution multispectral imagery. Some researchers have been working on change detection using high-spatial resolution imagery using object-oriented image segmentation techniques. For example, Walter (2004) performed an object-based change detection using pre-existing objects placed in a GIS database. His change detection method was based on maximum likelihood classification (MLC) and utilized input training data extracted from the GIS database. Blaschke (2005) dealt with the problems associated with multi-temporal object recognition using a post-classification comparison method and proposed a framework for image object-based change detection. Niemeyer *et al.* (2005) performed automation of change detection procedures based on a pixel-based multivariate alteration detection method with medium resolution imagery for simple 'change/no change' analysis, and an object-based procedure with high-resolution imagery for the detailed change information.

Deer (1998) introduced the notion of pixel, feature, and object-level image processing for change detection. The *pixel* level used brightness values or simple calculations between image bands such as image differencing. The *feature* level involved transformation of the spectral/spatial properties of the imagery using vegetation indices, principal component analysis, or other transformations. The *object* level referred to segments with spectral and spatial homogeneity within the imagery. Im and Jensen (2005) introduced local neighbourhood correlation image analysis and successfully generated *neighbourhood correlation images* (NCIs) consisting of three features (i.e. correlation, slope, and intercept) that improved classification for change detection. The NCIs improved the change detection results when compared with traditional per-pixel inputs. However, one of the problems found in the study was the 'salt-and-pepper' phenomenon in the change detection results, sometimes considered a drawback of per-pixel change detection (Blaschke and Strobl 2001). In addition, per-pixel approaches are often very sensitive to noise and therefore lack spatial consistency (Soille 2003).

This paper introduces an object-based correlation image analysis into the change detection process as an extension of the methodology discussed in Im and Jensen (2005). Three new input features, consisting of correlation, slope, and intercept, are generated using correlation analysis based on objects extracted through an image segmentation technique. These three new features are called *object correlation images* (OCIs). It is hypothesized that the OCIs might provide more useful information when detecting change than NCIs in the per-pixel high spatial domain due to several advantages of object-based analysis. The following processing steps were key elements in this research:

- OCIs were created based on the objects extracted using image segmentation and bi-temporal high-spatial resolution multispectral images.
- OCIs were compared with NCIs generated from the bi-temporal multispectral images using a 3×3 window.

- Composite images were classified by incorporating and excluding OCIs and/or NCIs according to machine-learning decision tree logic and nearest-neighbour classification logic, and the change detection results were evaluated.

2. Study area and data

2.1 *Study area*

Two Las Vegas study areas were used to demonstrate object-based change detection using object/neighbourhood correlation image analysis and image segmentation techniques. *Site A* is near downtown Las Vegas and documents residential development. *Site B* documents golf course development between two dates.

2.2 *Remote-sensor data*

QuickBird imagery from DigitalGlobe, Inc., acquired on 10 May 2002 and 18 May 2003, were used to detect change. Characteristics of the QuickBird remote sensor data are summarized in table 1. The panchromatic bands of *Site A* document residential development and the near-infrared bands of *Site B* document golf course development (figure 1).

2.3 *Remote-sensor data preprocessing*

Parallax was introduced into the bi-temporal datasets because each individual image was acquired at a slightly different off-nadir look angle and altitude (table 1). Orthorectification would normally be required to remove relief displacement. Fortunately, there were no tall buildings, and the ground was very level in the two study areas. Therefore, it was only necessary to geo-reference the datasets to a Universal Transverse Mercator (UTM) projection within an RMSE of 0.5 pixels based on the panchromatic bands and using nearest-neighbour resampling. Seasonal spectral variation was minimal, since both images were acquired on near-anniversary dates (10 May 2002 and 18 May 2003) and at about the same time (approximately 6:30 pm GMT). However, radiometric normalization of the bi-temporal data was necessary since the correlation analysis to be used directly compared the brightness values from the bi-temporal imagery. An empirical line calibration method (Jensen 2005) was used for radiometric normalization of the image datasets. This method included the collection of six pseudo-invariant water and bare soil radiometric ground control points. The individual 2002 bands were radiometrically normalized to the 2003 bands using the derived regression equations. Both panchromatic and multispectral images of different spatial resolutions were used in the subsequent analyses. A pan-sharpened process was not carried out, since the correlation image analysis required original brightness values. To avoid the discrepancy in spatial resolution between panchromatic and multispectral bands, the multispectral data were simply regenerated in 0.6×0.6 m pixel resolution for OCI generation and various change classifications (i.e. 16 pixels with same brightness values corresponded to one original multispectral pixel).

2.4 *Ground reference information*

A random sampling tool developed as a dynamic linked library (DLL) in Environmental Systems Research Institute (ESRI) ArcMap 9.1 using Visual Basic

Table 1. QuickBird satellite data characteristics and sensor position information of both datasets.

Acquisition date	Image size (pixels)	Spectral range (μm)(unit)		Spatial resolution (m)	Radiometric resolution (bits)	Acquisition time (GMT)	Off-nadir view angle	Sensor azimuth	Sensor elevation
10 May 2002	1408×1296* 2092×1568†	Band 1 Blue	0.45–0.52	2.4×2.4	11	18:26:31–35	12.8°	113.8°	76.1°
		Band 2 Green	0.52–0.60	2.4×2.4					
		Band 3 Red	0.63–0.69	2.4×2.4					
18 May 2003		Band 4 NIR	0.76–0.89	2.4×2.4		18:19:14–33	13.4°	164.2°	75.2°
		Band 5 PAN	0.45–0.90	0.6×0.6					

**Site A* (residential development, panchromatic band).
†*Site B* (golf-course development, panchromatic band).

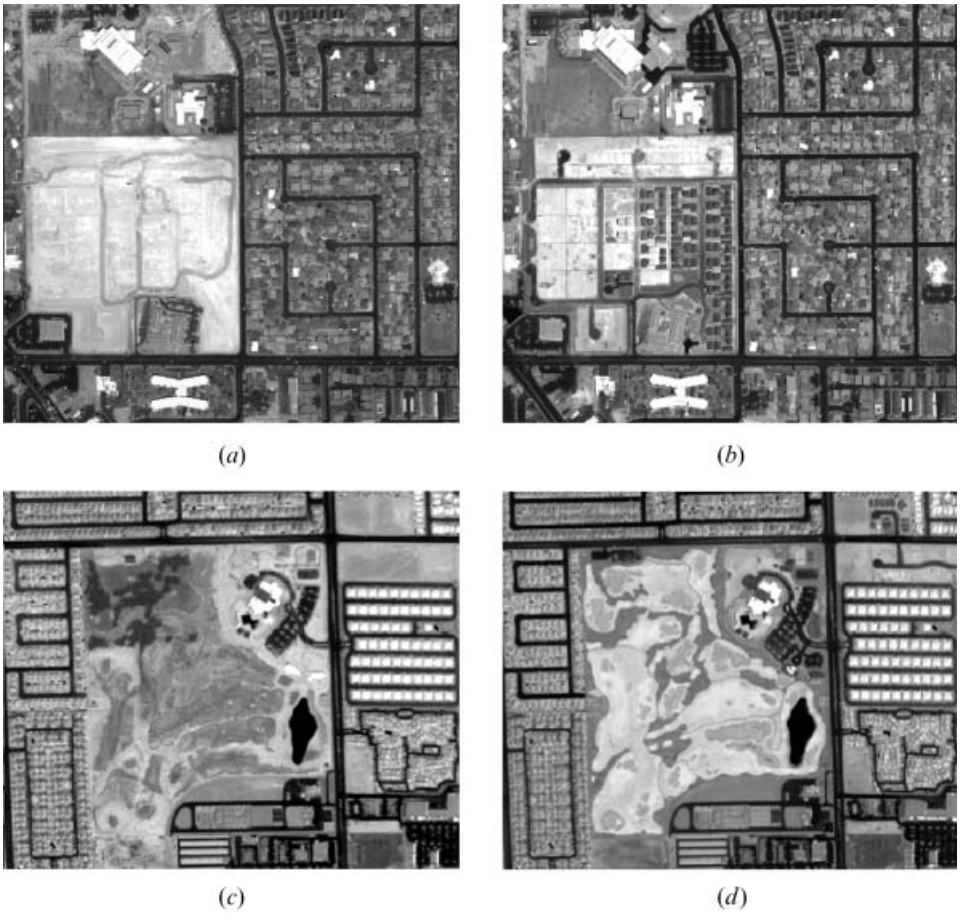

Figure 1. Two dates of imagery of the study sites: (*a*) and (*b*) are the panchromatic bands of QuickBird imagery for *Site A* (residential development) on 10 May 2002 and 18 May 2003, respectively, and (*c*) and (*d*) are the near-infrared bands of QuickBird imagery for *Site B* (golf course development) on 10 May 2002 and 18 May 2003, respectively. The near-infrared bands are presented for *Site B* to document the changes (i.e. from bare land to vegetation) more clearly.

(Im *et al.* 2005) was used to collect ground reference information to assess the accuracy of the various change classification methods. A total of 400 point samples were randomly generated within each study site. The land cover class of each sample location was identified based on the visual interpretation of the bi-temporal QuickBird imagery. Each reference point was assigned to one of eight classes:

- five unchanged classes: *water*, *built-up*, *paved road*, *bare land*, and *vegetation*
- three change classes: *bare land to built-up*, *bare land to paved road*, and *bare land to vegetation*.

Water was found in *Site B* only. The *built-up* class contained rooftops, buildings, and concrete materials. The *paved road* class consisted primarily of asphalt. The *Bare land* included bare soil and transitional areas. The *vegetation* class contained residential grass and trees, and golf course, fairways and greens. The three change

classes were areas that changed from bare ground into another land-use or land-cover category.

3. Methodology

This change detection research focused on how to incorporate the correlation analysis concept using bi-temporal imagery into object-based image processing (i.e. image segmentation). In order to generate correlation images based on objects by comparing brightness values from bi-temporal image datasets, a single set of image objects representing bi-temporal topology had to be created. Thus, two dates of imagery were used together in the segmentation procedure. Two different methods to incorporate correlation images into object-based change detection were examined.

The first method divided the bi-temporal imagery into meaningful objects and generated OCIs between bi-temporal imagery based on those objects. An object-based composite image consisting of the bi-temporal imagery (10 bands) plus the OCIs (three bands: object correlation, object slope, and object intercept) was created, followed by change classification to extract 'from–to' change information. Two classification algorithms were used: nearest-neighbour and machine-learning decision tree classifiers.

The second method generated NCIs between bi-temporal multispectral bands using a 3×3 window and created the composite imagery containing the bi-temporal image datasets (10 bands) plus the NCIs (three bands: neighbourhood correlation, neighbourhood slope, and neighbourhood intercept). Then, the composite imagery was divided into meaningful objects using image segmentation techniques. The same 'from–to' change classification of the object-based composite imagery followed using both nearest-neighbour and machine-learning decision tree classifiers. The steps associated with these two methods are summarized in figure 2.

Three additional methods were examined for comprehensive comparison. The third method excluded any additional features extracted from correlation analysis in change classification. In effect, it consisted of object-based classification based solely on the bi-temporal imagery. Thus, bi-temporal change classification using the panchromatic and multispectral data (10 bands) was performed using the two classification schemes. The fourth method incorporated pixel-based classification using the bi-temporal imagery plus the NCIs. The NCIs were first generated using a 3×3 neighbourhood, after which change classification based on the 13 bands composite imagery was performed using a machine-learning decision tree classifier. The fifth method consisted of traditional pixel-based classification with the exclusion of any additional contextual information. Pixel-based bi-temporal classification was performed using a machine-learning decision tree classifier. A brief summary of these five different methods is found in table 2.

3.1 *Object-oriented image segmentation*

Image objects were created using the image segmentation tool in *e*Cognition 4. The segmentation process in *e*Cognition 4 is a bottom-up region-merging approach, where the smallest objects contain single pixels (Baatz *et al.* 2004). In the process, smaller objects were merged into larger objects based on three parameters: scale, colour (spectral properties), and shape (smoothness and compactness). The segmentation process was stopped when the smallest growth of an object exceeded a user-defined threshold, which is an arbitrary value (i.e. a scale parameter) to

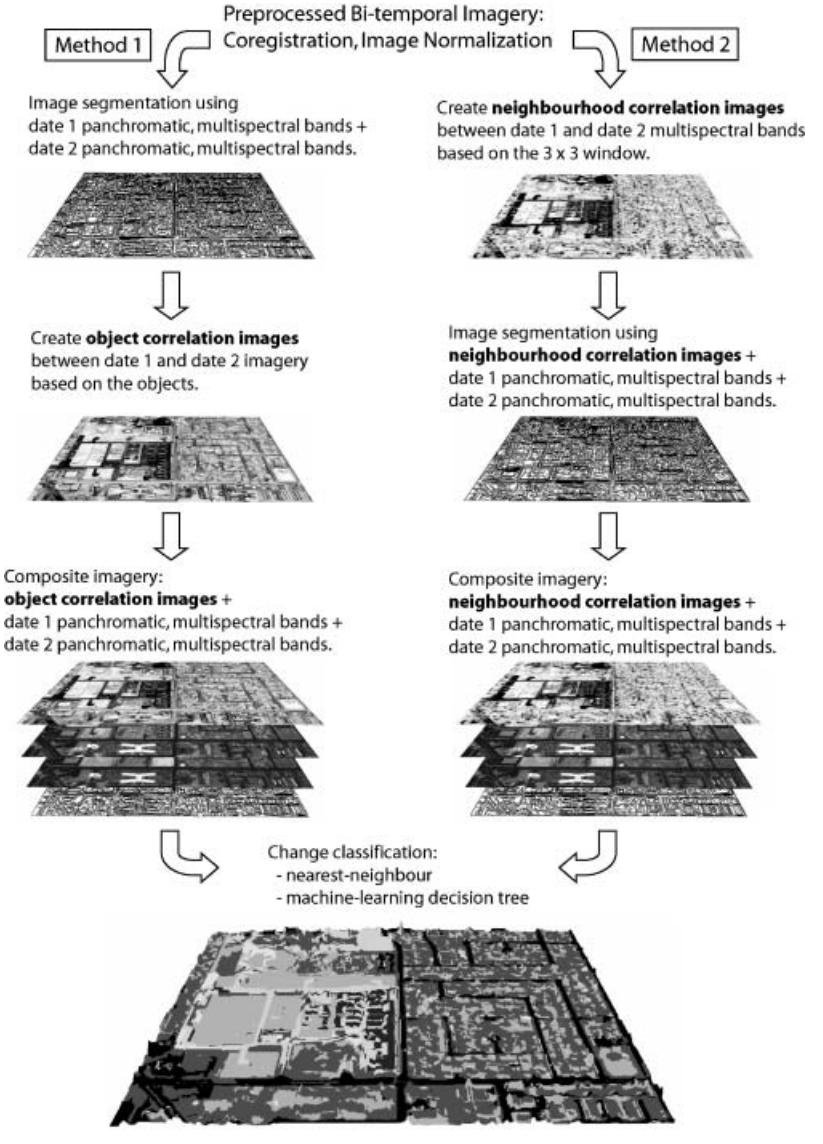

Figure 2. Flow diagram of two methodologies used in the study.

determine the maximum possible change in heterogeneity when several objects are merged (Benz *et al.* 2004). The greater the scale parameter, the larger the size of the resultant objects. A scale parameter of 60 (as applied to the panchromatic imagery with 0.6×0.6 m spatial resolution) was selected based on visual interpretation of the image segmentation results with different scale parameters. The value of 60 was considered appropriate to maximize both local homogeneity and global heterogeneity as well as to produce a reasonable number of objects to process.

The composition of homogeneity was controlled by both spectral and shape percentages as well as by a weight for the relative contribution of each input band. Spectral (colour) homogeneity was given an overall spectral factor percentage of 90%. Shape-homogeneity criteria included an overall shape factor percentage of 10%

Table 2. Five different change detection methods used in the study.

Method	Process description
Method 1	• Generate objects through image segmentation (using two dates of PAN + MS) • Create object correlation images based on the objects (between two dates of PAN + MS) • Classify the object-based composite imagery (OCIs + date 1 PAN, MS + date 2 PAN, MS) ○ nearest-neighbour (NN) ○ machine-learning decision tree (DT)
Method 2	• Create neighbourhood correlation images (between two dates of MS bands) • Generate objects through image segmentation (using NCIs + two dates of PAN, MS) • Classify the object-based composite imagery (NCIs + date 1 PAN, MS + date 2 PAN, MS) ○ nearest-neighbour (NN) ○ machine-learning decision tree (DT)
Method 3	• Generate objects through image segmentation (using two dates of PAN + MS) • Classify the object-based composite imagery (date 1 PAN, MS + date 2 PAN, MS) ○ nearest-neighbour (NN) ○ machine-learning decision tree (DT)
Method 4	• Create neighbourhood correlation images (between two dates of MS bands) • Classify the composite imagery (NCIs + date 1 PAN, MS + date 2 PAN, MS) ○ machine-learning decision tree (DT)
Method 5	• Classify the composite imagery (date 1 PAN, MS + date 2 PAN, MS) ○ machine-learning decision tree (DT)

which was subdivided into smoothness (8%) and compactness (2%). A higher compactness value helps separate objects with different shapes but not necessarily much colour contrast (e.g. rooftops versus roads), while a higher smoothness weight helps identify objects that have a greater variability between features (Baatz *et al.* 2004, Syed *et al.* 2005). Finally, equal weight was assigned to each of the input bands in Methods 1 through 3 (where image segments were computed). All parameters set during the image segmentation procedure were selected through a trial-and-error method. Several combinations of the parameters were tested, and one optimum set of the parameters was selected based on visual inspection of the resultant polygonal data. A total of 10 bands from the bi-temporal image datasets were input for image segmentation processes in Methods 1 and 3, while 13 bands from bi-temporal image datasets plus the NCIs (correlation, slope, and intercept) were input for the image segmentation process in Method 2 (table 2).

Objects extracted from the image segmentation process contained new spectral and spatial information including *difference to neighbours*, *shape information*, *texture*, *hierarchy*, as well as *mean brightness values*. Many object-based studies have not utilized this variety of object-related information. This might be because the procedure to use such information (e.g. shape) is not simple, and in most cases, users must define directly the relationship with the information (e.g. membership function). In this study, only *mean* layer values were used in the subsequent change classification based on a machine-learning decision tree or nearest-neighbour classifiers. In the context of the added complexity of these change detection experiments, this decision resulted in simplicity and consistency between the methods.

3.2 *Objectlneighbourhood correlation image analysis*

This study incorporated spectral contextual information (i.e. correlation, slope, and intercept) extracted from correlation analysis based on objects and/or local neighbourhoods between two dates. Correlation image analysis is based on the *change magnitude* and *direction* of brightness values by band in an object or a specified neighbourhood between two multispectral remote sensing datasets. If the spectral changes in pixels within the object or neighbourhood between two image dates were significant, then the contextual variables provided unique change information in the form of a lower correlation coefficient or a variable slope/intercept (Im and Jensen 2005).

Correlation analysis was used to detect change based on the objects derived from image segmentation and the 3×3 local neighbourhood. A more detailed explanation of the correlation image analysis used for change detection can be found in Im and Jensen (2005). Three variables—correlation, slope, and intercept—from the correlation analysis were calculated using the following equations (Im and Jensen 2005):

$$r = \frac{\sum_{i=1}^{n} (\mathrm{BV}_{i1} - \mu_1)(\mathrm{BV}_{i2} - \mu_2)}{s_1 s_2 (n-1)} \tag{1}$$

$$a = \frac{\sum_{i=1}^{n} (\mathrm{BV}_{i1} - \mu_1)(\mathrm{BV}_{i2} - \mu_2)}{s_1^2 (n-1)} \tag{2}$$

$$b = \frac{\sum_{i=1}^{n} \mathrm{BV}_{i2} - a \sum_{i=1}^{n} \mathrm{BV}_{i1}}{n} \tag{3}$$

where r is Pearson's product-moment correlation coefficient, and s_1 and s_2 are the standard deviations of the brightness values found in all bands of each dataset in the object/neighbourhood, respectively. BV_{i1} is the ith brightness value of the pixels found in all bands of image 1 in the object/neighbourhood, BV_{i2} is the ith brightness value of the pixels found in all bands of image 2 in the object/neighbourhood, n is the total number of the pixels found in all bands of each dataset in the object/neighbourhood, and μ_1 and μ_2 are the means of brightness values found in all bands of the two date (1 and 2) images in the object/neighbourhood, respectively.

Based on the above basic equations, *object correlation images* (OCIs) were created using the following spatial analysis:

- correlation image:

$$\frac{N \times B \times \sum_{i=1}^{B} ZD1D2_i - \left(\sum_{i=1}^{B} ZD1_i \times \sum_{i=1}^{B} ZD2_i\right)}{\sqrt{\left(N \times B \times \sum_{i=1}^{B} ZD12_i - \left(\sum_{i=1}^{B} ZD1_i\right)^2\right) \times \left(N \times B \times \sum_{i=1}^{B} ZD22_i - \left(\sum_{i=1}^{B} ZD2_i\right)^2\right)}} \tag{4}$$

- slope image:

$$\frac{N \times B \times \sum_{i=1}^{B} ZD1D2_i - \left(\sum_{i=1}^{B} ZD1_i \times \sum_{i=1}^{B} ZD2_i\right)}{N \times B \times \sum_{i=1}^{B} ZD12_i - \left(\sum_{i=1}^{B} ZD1_i\right)^2} \tag{5}$$

- intercept image:

$$\frac{\sum_{i=1}^{B} ZD2_i - \mathrm{SI} \times \sum_{i=1}^{B} ZD1_i}{N \times B} \tag{6}$$

where N is the image containing the number of cells in each object (zone), and B is the number of bands in one date of imagery. $ZD1_i$ and $ZD2_i$ are the images generated using a zonal sum function (based on the polygonal zone vector data) of band i of date 1 and date 2 imagery, respectively. $ZD1D2_i$ is the image generated using a zonal sum function (based on the polygonal zone vector data) of the image generated by multiplying band i of date 1 imagery with band i of date 2 imagery. $ZD12_i$ and $ZD22_i$ are the images generated using a zonal sum function (based on the polygonal zone vector data) of the images generated by multiplying band i of each date imagery by itself, respectively. SI is the slope image from equation (5). A data-processing flow diagram for the generation of *object correlation images* (OCIs) is shown in figure 3. Generating *neighbourhood correlation images* (NCIs) followed a similar process. The only difference was that neighbourhood information (e.g. 3×3 window) was used in the spatial analysis (4) through (6), instead of the zonal (object) information. The tools for creating OCIs and NCIs were developed as a dynamic linked library (DLL) in ESRI ArcMap 9.1 using Visual Basic.

3.3 *Classification algorithms*

Two algorithms were used to classify the composite imagery, including a machine-learning decision tree classifier and a nearest-neighbour classifier. Machine-learning decision trees have gained significant momentum in geocomputation application (e.g. Huang and Jensen 1997, Muchoney *et al.* 2000, Hodgson *et al.* 2003, Jensen 2005), largely due to their simplicity and speed for predicting numbers (regression) or classes (classification) from example data. Machine-learning decision tree classification was successfully used in the Im and Jensen (2005) study. In classification literature, machine-learning decision tree classifiers are considered non-metric (as opposed to parametric or non-parametric) due to their use of heuristics. Through these heuristics (whether published or proprietary), they have several advantages over traditional statistical techniques, including that they make no assumptions about data distribution and independency (Quinlan 2003, Jensen 2005).

Quinlan's C5.0 (RuleQuest Research, 2005) inductive machine-learning decision tree was used in this study. Although not designed specifically for digital image

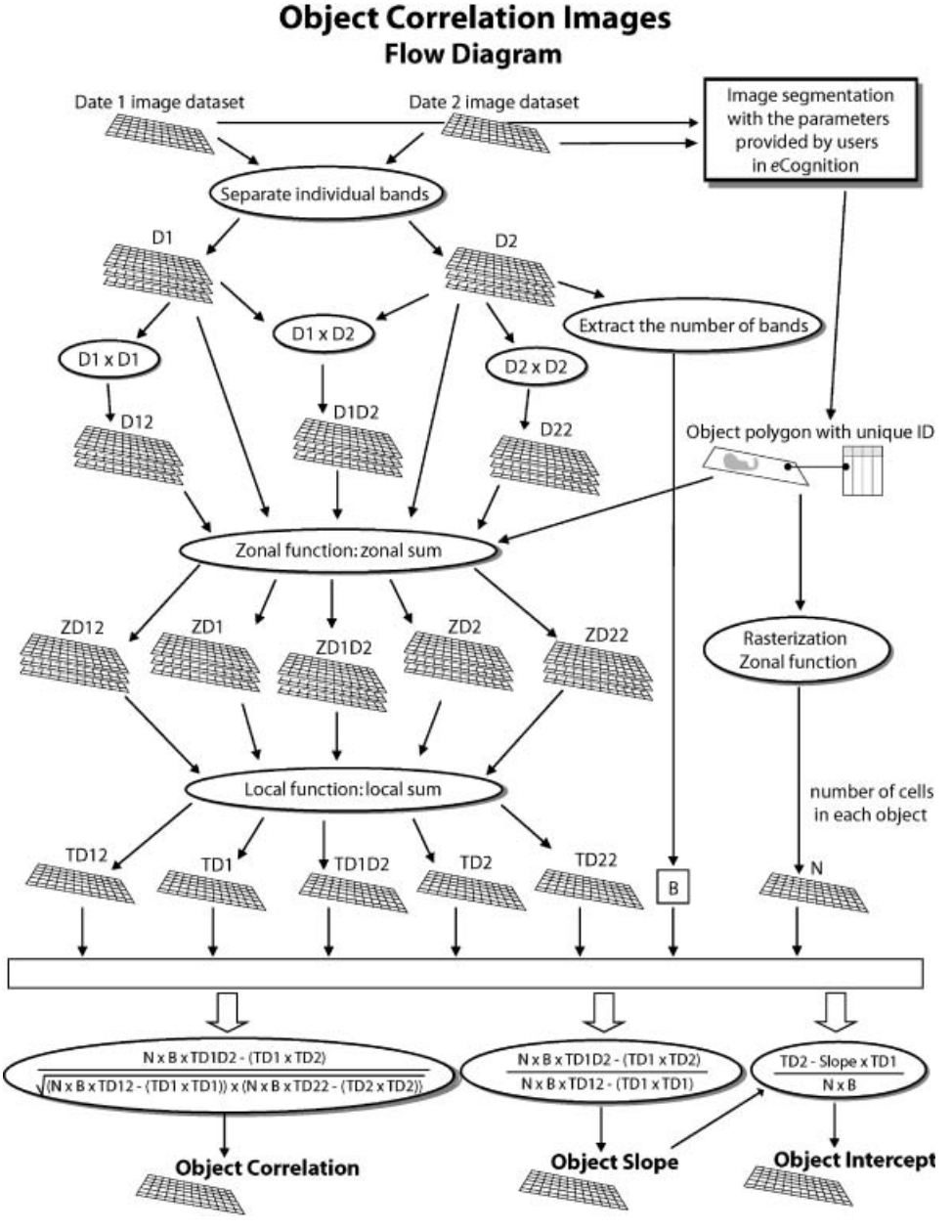

Figure 3. Flow diagram for the creation of *object correlation images* (OCIs).

processing, C5.0 has been widely used in remote sensing classification (Huang and Jensen 1997, Hodgson *et al.* 2003, Tullis and Jensen 2003, Im and Jensen 2005). Jensen (2005) summarizes the logic used by the C5.0 decision tree classifier:

1. C5.0 utilizes a recursive 'divide and conquer' strategy to generate a decision tree from a training dataset.
2. The most efficient attributes are selected at each node of the decision tree based on the entropy concept from communications theory (an attribute with

minimal entropy has, on average, more unique information than attributes of higher entropy and is therefore best suited for dividing the dataset into separate groups).

3. The C5.0 generated decision tree (often difficult to read and understand) is converted to production rules (a series of if–then statements).
4. Because of the nature of definitive production rules, a major challenge is that the rules do not necessarily cease to be mutually exclusive or collectively exhaustive. Rule confidences and a default class are utilized in a voting procedure that ensures that rule inferences can be successful in cases where they do not provide definitive answers.

The tool developed for this study was built to apply the C5.0 outputs in either format (i.e. decision trees or production rules) to the corresponding imagery. It was also implemented as a DLL in ESRI ArcMap 9.1 using Visual Basic. Both formats were produced with the training samples in Methods 1–5. In most cases, the decision-tree outputs resulted in slightly better performance than the production rules with the training cases. Thus, the decision-tree outputs were applied to the corresponding imagery.

As a default object-based classification method in *e*Cognition, the nearest-neighbour algorithm was selected as an alternative technique for change classification. The standard nearest-neighbour algorithm in *e*Cognition computes the Euclidean distance from the object to be classified to the nearest training object and assigns it to the class of the training object. Again, the layer *mean* values were used in the nearest-neighbour classification in *e*Cognition. In both classification techniques (i.e. machine-learning decision tree and nearest-neighbour), collecting training data was necessary. For a reasonable comparison between the change detection results, the same training data were used in the classification. First, 600–700 (stratified random) point samples were generated for each study site through visual inspection with at least 10 points per class. Layer values of those points (i.e. layer *mean* values in the segments for Methods 1–3, pixel brightness values for Methods 4 and 5) in the composite imagery were used as inputs in the machine-learning decision tree logic classifications. The polygonal objects containing the point samples were extracted from the composite imagery and used as training samples in the nearest-neighbour classification in *e*Cognition.

A total of 16 composite image datasets were prepared for change classifications: 12 composite images for Methods 1–3 (four per method), and four composite images for Methods 4 and 5 (two per method). Object-based classifications were carried out in Methods 1–3 only (table 3).

3.4 *Accuracy assessment*

An accuracy assessment was accomplished for the 16 change classifications based on seven land-cover classes for *Site A* and eight land-cover classes for *Site B*. In each case, the accuracy assessment included the user's (errors of omission) and producer's (errors of commission) accuracy, overall accuracy, and the Kappa coefficient of agreement. In addition, a *Z*-test was performed to test for differences between the eight Kappa coefficients for each site (Congalton and Green 1999, Gwet 2002).

Table 3. Summary of a total of 16 change classifications.

Method	Classification algorithm	Study site*	Designation†	Total no. of bands in composite imagery
Method 1	Nearest-neighbour	A	M1NNA	13 (including OCIs)
	Nearest-neighbour	B	M1NNB	13 (including OCIs)
	Machine-learning decision tree	A	M1DTA	13 (including OCIs)
	Machine-learning decision tree	B	M1DTB	13 (including OCIs)
Method 2	Nearest-neighbour	A	M2NNA	13 (including NCIs)
	Nearest-neighbour	B	M2NNB	13 (including NCIs)
	Machine-learning decision tree	A	M2DTA	13 (including NCIs)
	Machine-learning decision tree	B	M2DTB	13 (including NCIs)
Method 3	Nearest-neighbour	A	M3NNA	10 (bi-temporal imagery)
	Nearest-neighbour	B	M3NNB	10 (bi-temporal imagery)
	Machine-learning decision tree	A	M3DTA	10 (bi-temporal imagery)
	Machine-learning decision tree	B	M3DTB	10 (bi-temporal imagery)
Method 4	Machine-learning decision tree	A	M4DTA	13 (including NCIs)
	Machine-learning decision tree	B	M4DTB	13 (including NCIs)
Method 5	Machine-learning decision tree	A	M5DTA	10 (bi-temporal imagery)
	Machine-learning decision tree	B	M5DTB	10 (bi-temporal imagery)

*A: residential development; B: golf course development.
†M1–M5 indicate the five different methods; NN represents nearest-neighbour classification, while DT represents decision tree classification; A and B represent the two study sites.

4. Results and discussion

4.1 *Comparison between OCIs and NCIs*

Object correlation images were generated from bi-temporal panchromatic plus multispectral imagery based on the objects extracted using an image segmentation technique. Thus, the spatial resolution of the OCIs was 0.6×0.6 m, which is the same as that of the panchromatic bands. Conversely, *neighbourhood correlation images* were generated from the bi-temporal multispectral imagery (excluding the panchromatic bands) using a 3×3 window, which resulted in NCIs with a 2.4×2.4 m spatial resolution, the same resolution of the multispectral bands. A scale parameter of 60 was used in the image segmentation procedure, and this produced relatively large objects, containing more pixels than those within the local 3×3 neighbourhood. Since the OCIs were generated using more cells in the correlation calculation, it was expected that the NCIs would show more variation than the OCIs.

The generated OCIs and NCIs are shown in figure 4 where (*a*), (*c*), and (*e*) are the object correlation, slope, and intercept images, respectively, and (*b*), (*d*), and (*f*) are the neighbourhood correlation, slope, and intercept images, respectively. Visual

Figure 4. Object correlation images, (*a*), (*c*), and (*e*), vs. neighbourhood correlation images, (*b*), (*d*), and (*f*) for *Site B* (golf course development). (*a*) Object correlation image; (*b*) neighbourhood correlation image; (*c*) object slope image; (*d*) neighbourhood slope image; (*e*) object intercept image; (*f*) neighbourhood intercept image.

inspection suggests that both processes produced similar outputs. Since the OCIs were generated based on objects, the 'salt-and-pepper' problem that was easily detected in the NCIs was eliminated. NCIs with larger neighbourhoods (e.g. 9×9 window), which reduced the 'salt-and-pepper' problem (Im and Jensen 2005) might produce results similar to those of the OCIs. However, the NCIs with larger neighbourhoods could conceivably alter the change information; for example, they could overestimate change or miss linear change such as new narrow roads (Im and

Jensen 2005). On the other hand, OCIs can remove the errors that are likely to occur in the NCIs with larger neighbourhoods.

The brighter the pixel in a correlation image, the higher the correlation (figures 4(*a*) and 4(*b*)). Referring to the original imagery, the correlation image seemed to detect change quite well. In the slope and intercept images, the unchanged pixels are generally shown in mid-grey tones, while the pixels with the brighter or the darker colours have a greater likelihood of change.

Figure 5 compares the distribution between OCI and NCI variables based on the 400 *Site B* ground reference checkpoints. From the correlation graph (figure 5(*a*)), the distribution of the object correlations is similar to that of the neighbourhood correlations in all land cover classes. As expected, most correlation values of the unchanged classes in either object or neighbourhood images were higher than 0.8, while the changed classes exhibited lower correlations. However, note that a few reference points of the *bare land to built-up* class exhibited a relatively high correlation ($\sim$0.8). Nevertheless, the change classes with high correlation values were easily separated from the unchanged classes by incorporating slope and intercept values. For example, the slope and the intercept values of the *bare land to built-up* class were generally below 0.5 and over 100, respectively (figures 5(*b*) and 5(*c*)), which makes them easily separable from the unchanged classes.

The distribution of the object slopes was also similar to that of the neighbourhood slopes in most land cover classes. The object slope values in the *paved road* class showed a much smaller variance than the neighbourhood slope values. The same distributions of the correlation and intercept values were evident in the *paved road* class. One reason for this is that the local neighbourhood may not function well in the linear features such as long narrow roads. In other words, most objects found in the paved road have linear (long and narrow) shapes along the roads, unlike compact shapes found in other land cover classes or a 3×3 neighbourhood. The lower spatial resolution of the NCIs (2.4×2.4 m) might also affect such large variance in the *paved road* class. Most slope values in the unchanged classes in either the object or neighbourhood image range from 0.8 to 1, while the change classes had slope values <0.8 (figure 5(*b*)). The distribution of the object intercepts was also similar to that of the neighbourhood intercepts in most land cover classes. Most intercept values of the unchanged classes either in the object or neighbourhood image range from -50 to 100 except in the *built-up* class which had intercept values from 50 to 150, while the change classes generally had higher intercept values >100 (figure 5(*c*)). Like the slope comparison, the distribution of the neighbourhood intercepts has a larger variance than that of the object intercepts. All classes except the *bare land to vegetation* exhibited lower neighbourhood intercept values compared with the object intercepts. Ideally, if there was no change, pairs of brightness values between the two dates of imagery would have higher correlation coefficients, slopes around 1, and intercepts around 0.

Atmospheric effects may influence slope and intercept values even when radiometric correction has been performed. The remnant atmospheric effects in the bi-temporal datasets after radiometric correction can be easily identified from the distribution of the slope and intercept values of the unchanged classes. For example, the slope values of the unchanged classes ranged from 0.7 to 1.1, not exactly symmetrical to 1 (figure 5(*b*)). If the atmospheric effects are perfectly removed between bi-temporal datasets, distribution of slope values in unchanged area should be symmetrical to 1, while intercept values in the area should be

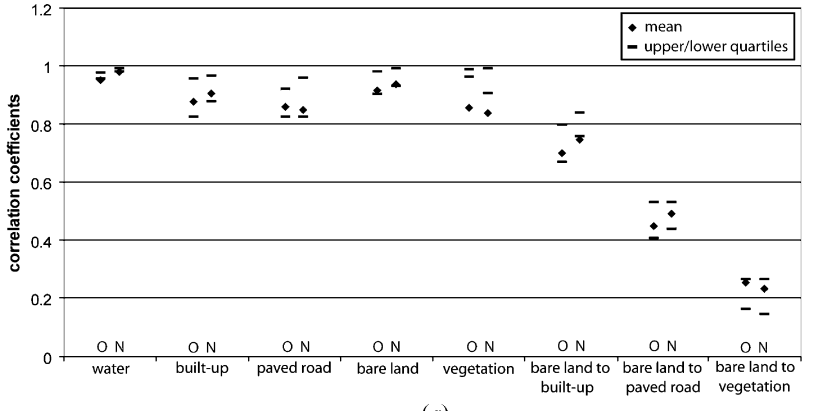

(*a*)

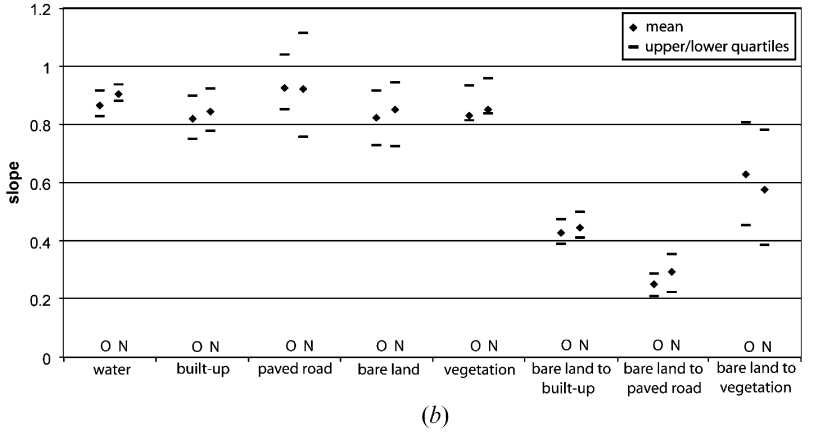

(*b*)

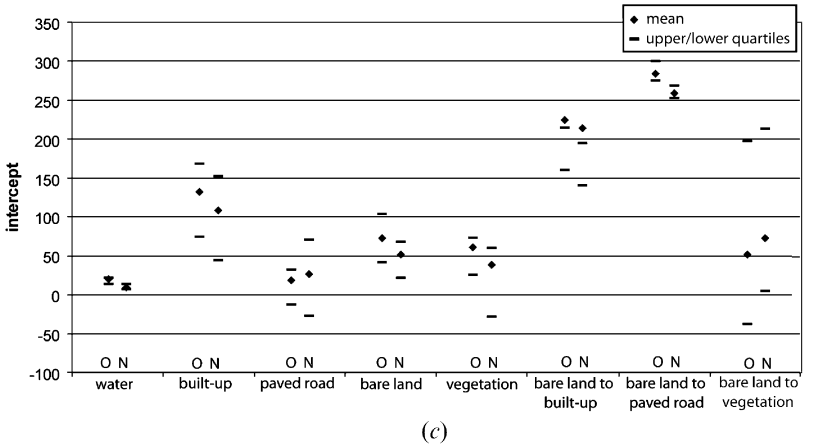

(*c*)

Figure 5. Graphical comparison between the OCI and NCI variables based on the 400 reference data for *Site B*: (*a*) correlation comparison; (*b*) slope comparison; (*c*) intercept comparison. O: statistics were computed from the OCIs. N: statistics were computed from the NCIs.

Table 4. Statistical analysis results for comparison between OCI and NCI variables based on 400 reference data for *Site B**.

Classes	Statistics	Variables (OCIs vs. NCIs)		
		Correlation	Slope	Intercept
Water	*t*-statistic	−1.582	−1.418	**2.210**
	Pr>*t*	0.1356	0.1739	**0.0407**
Built-up	*t*-statistic	**−2.352**	−1.892	**1.964**
	Pr>*t*	**0.0195**	0.0597	**0.0507**
Paved road	*t*-statistic	0.644	0.236	−0.741
	Pr>*t*	0.5211	0.8142	0.4599
Bare land	*t*-statistic	−1.183	−0.985	**2.427**
	Pr>*t*	0.2390	0.3265	**0.0166**
Vegetation	*t*-statistic	1.017	−0.461	1.024
	Pr>*t*	0.3159	0.6477	0.3129
Bare land to built-up	*t*-statistic	−0.695	−0.325	0.197
	Pr>*t*	0.4928	0.7475	0.8455
Bare land to paved road	*t*-statistic	−1.132	−1.179	**2.682**
	Pr>*t*	0.2701	0.2534	**0.0144**
Bare land to vegetation	*t*-statistic	0.978	1.267	−0.643
	Pr>*t*	0.3295	0.2073	0.5215

*Values in bold indicate a rejection of the null hypothesis (there is no difference between the OCI and NCI variables) based on a 95% confidence level.

symmetrical to 0. Different look angles of bi-temporal high-spatial resolution imagery may also influence the distribution of slope and intercept variables.

Statistical *t*-tests with the reference data for *Site B* were performed to determine if there were any significant differences between the OCI and NCI variable group means (table 4). In most cases, there was no statistically significant difference between the OCI and NCI means. However, the mean of the neighbourhood correlation distribution in the *built-up* class was statistically higher than that of the object correlation values based on a 95% confidence level. Compared with other classes showing similar distributions, this significance might be due to the relatively large sample size of the *built-up* class (123 out of 400). The means of the object intercepts in the *water*, *built-up*, *bare land*, *bare land to built-up*, and *bare land to paved road* classes were statistically higher than those of the neighbourhood intercept values based on a 95% confidence due to relatively large variances of both intercept variables. The use of the objects with smaller scale sizes during the image segmentation process (e.g. 15) might produce results more similar to the NCIs.

4.2 *Change classification*

The generated OCIs and NCIs were used in the subsequent change classifications and were expected to provide somewhat unique change information. Tables 5 and 6 summarize the accuracy assessment associated with the 16 change classifications: eight classifications for seven classes associated with the 400 reference data for *Site A*, and eight classifications for eight classes associated with the 400 reference data for *Site B*.

The change classification using the bi-temporal image datasets plus the OCIs based on the machine-learning decision tree logic for *Site A* (i.e. M1DTA from table 3) exhibited the highest classification accuracy with an overall accuracy of 91% and a Kappa of 89% (table 5). The change classification using the bi-temporal image

Table 5. Accuracy assessment of the 16 change classifications for *Site A*.

		Unchanged classes				Change classes		
Category	Accuracy†	*Built-up*	*Paved road*	*Bare land*	*Vegetation*	*Bare land to built-up*	*Bare land to paved road*	*Bare land to vegetation*
M1DTA	PA	88.98	90.79	91.07	84.09	92.68	97.14	100
	UA	87.5	94.52	86.44	94.87	100	85	96.77
	OA				91			
	Kappa				89.0			
M2DTA	PA	88.98	80.26	91.07	90.91	82.93	91.43	96.67
	UA	86.78	93.85	85	97.56	94.44	**72.73**	87.88
	OA				88			
	Kappa				85.4			
M3DTA	PA	80.51	**78.95**	89.29	88.64	87.81	88.57	90
	UA	86.36	90.91	89.29	92.86	92.31	**54.39**	90
	OA				84.5			
	Kappa				81.3			
M4DTA	PA	80.51	94.74	92.86	88.64	85.37	**68.57**	100
	UA	89.62	88.89	**77.61**	97.5	**79.55**	80	93.75
	OA				86.75			
	Kappa				83.9			
M5DTA	PA	**77.12**	85.53	91.07	90.91	85.37	**77.14**	83.33
	UA	89.22	89.04	83.61	97.56	81.40	**51.92**	89.29
	OA				83.5			
	Kappa				80.1			
M1NNA	PA	92.37	85.53	89.29	93.18	87.81	85.71	100
	UA	88.62	98.49	90.91	95.35	85.71	**76.92**	93.75
	OA				90.25			
	Kappa				88.1			
M2NNA	PA	88.14	89.47	94.64	90.91	82.93	88.57	100
	UA	92.86	91.89	88.33	100	87.18	**72.09**	93.75
	OA				90			
	Kappa				87.9			
M3NNA	PA	87.29	85.53	83.93	90.91	85.37	**65.71**	100
	UA	89.57	95.59	83.93	95.24	**72.92**	**63.89**	85.71
	OA				85.75			
	Kappa				82.7			

*Values in bold indicate accuracy <80%. All accuracies are presented as a percentage.
†PA: producer's accuracy; UA: user's accuracy; OA: overall accuracy.

datasets plus the OCIs based on the nearest-neighbour logic for *Site A* (i.e. M1NNA from table 3) produced the second highest classification accuracy with an overall accuracy of 90.25% and a Kappa of 88.1%. The change classification using the bi-temporal image datasets plus the NCIs based on the nearest-neighbour logic (i.e. M2NNA) exhibited an overall accuracy of 90% and a Kappa of 87.9%, followed by the change classification using the bi-temporal image datasets plus the NCIs based on the decision-tree logic (i.e. M2DTA: an overall accuracy of 88% and a Kappa of 85.4%). The lowest classification accuracy for *Site A* was found in M5DTA (i.e. traditional per-pixel classification without any additional features based on the machine-learning decision tree logic) with an overall accuracy of 83.5% and a Kappa of 80.1%. In most change classifications for *Site A*, the *bare land to paved road* class was somewhat confused with many pixels in the class misclassified as *bare land to the built-up*. There was also some confusion between the *built-up* and *paved road* classes.

Table 6. Accuracy assessment of the 16 change classifications for *Site B*.

		Unchanged classes					Change classes		
Category	Accuracy*	Water	*Built-up*	*Paved road*	*Bare land*	*Vegetation*	*Bare land to built-up*	*Bare land to paved road*	*Bare land to vegetation*
M1DTB	PA	100	87.81	96.25	90.63	95	86.67	91.67	100
	UA	100	93.10	95.06	81.69	100	86.67	100	98.67
	OA					93			
	Kappa					91.3			
M2DTB	PA	100	91.87	98.75	81.25	95	80	91.67	100
	UA	100	89.68	92.94	91.23	90.48	85.71	100	100
	OA					93			
	Kappa					91.2			
M3DTB	PA	100	80.49	96.25	**70.31**	95	86.67	91.67	100
	UA	100	84.62	95.06	**72.58**	95	**56.52**	100	100
	OA					87.5			
	Kappa					84.5			
M4DTB	PA	100	81.30	97.5	87.5	95	80	91.67	98.59
	UA	100	90.91	96.30	**76.71**	95	**66.67**	84.62	100
	OA					90.25			
	Kappa	87.9							
M5DTB	PA	100	**77.24**	96.25	**64.06**	90	**73.33**	91.67	100
	UA	100	**79.83**	97.47	**62.12**	100	**61.11**	84.62	98.67
	OA					84.75			
	Kappa					81.0			
M1NNB	PA	100	91.87	95	**79.69**	95	93.33	100	100
	UA	100	91.87	96.20	86.44	100	**63.64**	100	100
	OA					92.75			
	Kappa					91.0			
M2NNB	PA	100	91.87	96.25	84.38	90	93.33	91.67	100
	UA	100	91.13	97.47	90	100	**63.64**	100	100
	OA					93.25			
	Kappa					91.6			
M3NNB	PA	100	82.11	96.25	**67.19**	100	86.67	83.33	100
	UA	100	84.87	97.47	**68.25**	100	**56.52**	100	100
	OA					87.5			
	Kappa					84.4			

*Values in bold indicate accuracy <80%. All accuracies are presented as a percentage.
†PA: producer's accuracy; UA: user's accuracy; OA: overall accuracy.

The highest classification accuracy for *Site B* was found in the nearest-neighbour classification incorporating the NCIs (i.e. M2NNB), with an overall accuracy of 93.25% and a Kappa of 91.6%. The change classification incorporating the OCIs based on the decision tree logic (i.e. M1DTB) exhibited the second highest classification accuracy with an overall accuracy of 93% and a Kappa of 91.3%, followed by M2DTB (an overall accuracy of 93% and a Kappa of 91.2%) and M1NNB (an overall accuracy of 92.75% and a Kappa of 91.0%). The lowest classification accuracy was produced by M5DTB with an overall accuracy of 84.75% and a Kappa of 81.0%. The greatest degree of misclassification occurred between the *bare land* and *bare land to built-up* classes (table 6).

In both *Sites A* and *B*, Methods 1 and 2 that incorporated the OCIs or the NCIs into change classifications produced useful classification results, which indicated that the three new feature variables (i.e. correlation, slope, and intercept) in either

object or neighbourhood provided unique change information in the classification process. Methods 3 and 5 that did not incorporate any additional contextual features in the classification process produced relatively lower classification accuracies (ranked the lowest three classification accuracies for each site: M3NNA, M3DTA, and M5DTA; M3DTB, M3NNB, and M5DTB). Method 3, a per-pixel analysis incorporating the NCIs into the classification process, yielded the higher classification accuracy between the above two groups. Table 7 summarizes the Kappa analysis between the eight change classifications based on seven land-cover classes for *Site A*, and between the eight change classifications based on eight land-cover classes for *Site B*. From the *Z*-test between the Kappas, some of the change classifications incorporating the OCIs or the NCIs were significantly more accurate than the classification without any contextual features when the same classification algorithm (machine-learning decision tree or nearest-neighbour) and type (object-based or pixel-based) were applied (e.g. significant: M1DTA vs. M3DTA; not significant: M2DTA vs. M3DTA).

Two different classification algorithms were applied in the research: machine-learning decision tree and nearest-neighbour. There was little difference in the classification results (tables 5 and 6) between these two classification algorithms applied when the other conditions were held constant (e.g. M1DTA vs. M1NNA; M2DTB vs. M2NNB). This may be because the two classifications were carried out with the averaged brightness values per object, which caused the heterogeneity in spectral properties of the original imagery to be considerably reduced in the object-based data through the image segmentation process. Thus, the machine-learning decision tree logic did not function much better than the simple nearest-neighbour classifier. From the *Z*-test between the Kappas (table 7), there was no significant difference between the machine-learning decision tree and nearest-neighbour classifications when the same classification type (object-based or pixel-based) and additional contextual features (OCIs or NCIs) were applied (e.g. M1DTA vs. M1NNA).

The object-based classifications produced higher classification accuracies than the pixel-based classifications (tables 5 and 6). However, the differences in the classification accuracies between the object-based and pixel-based classifications were not statistically significant from the *Z*-test between the Kappa coefficients (table 7) when the same classification algorithm (machine-learning decision tree or nearest-neighbour) and additional contextual features (OCIs or NCIs) were applied (e.g. M1DTA/M2DTA vs. M4DTA).

Figure 6 documents the four select classification outputs: the best ((*a*) and (*c*)) and worst ((*b*) and (*d*)) classifications for *Site A* and *B*, respectively. The 'salt-and-pepper' phenomenon can be detected in the M5DTA and M5DTB pixel-based change classifications, while the noise was reduced in the M1DTA and M2NNB object-based change classifications. The *built-up* class seemed dominant in M1DTA and M2NNB, possibly due to relatively large training samples of the class. Another reason for this is that the resolution of the multispectral bands (i.e. 2.4×2.4 m) may not be sufficient for detecting small non-built-up areas within the residential areas. Such areas were mixed with nearby built-up areas in the 2.4×2.4 m resolution and were classified as the *built-up* class. The *vegetation* class seemed to be overestimated in the M5DTA treatment, and the *bare land* class was overestimated in M5DTB, compared with M1DTA and M2NNB, respectively. In all classifications, most errors occurred in the boundaries of the artefacts (e.g. houses) or natural materials (e.g. trees) found in the scene probably due to the parallax introduced in the image datasets.

Table 7. Kappa *Z*-test analysis based on the change detection results for *Site A* and *Site B*.

Classification	ASE	M1DTA	M2DTA	M3DTA	M4DTA	M5DTA	M1NNA	M2NNA	M3NNA
Site A									
M1DTA	0.0175	NA							
M2DTA	0.0198	1.373	NA						
M3DTA	0.0219	**2.766**	1.397	NA					
M4DTA	0.0206	1.886	0.515	0.883	NA				
M5DTA	0.0224	**3.139**	1.771	0.374	1.257	NA			
M1NNA	0.0181	0.361	1.014	**2.409**	1.528	**2.783**	NA		
M2NNA	0.0182	0.461	0.917	**2.314**	1.432	**2.689**	0.099	NA	
M3NNA	0.0211	**2.303**	0.928	0.474	0.412	0.848	1.944	1.848	NA
Site B									
M1DTB	0.016	NA							
M2DTB	0.016	0.018	NA						
M3DTB	0.0207	**2.604**	**2.588**	NA					
M4DTB	0.0185	1.377	1.360	1.241	NA				
M5DTB	0.0226	**3.713**	**3.698**	1.132	**2.367**	NA			
M1NNB	0.0162	0.136	0.118	**2.474**	1.243	**3.586**	NA		
M2NNB	0.0157	0.135	0.153	**2.739**	1.513	**3.846**	0.272	NA	
M3NNB	0.0207	**2.611**	**2.595**	0.006	1.247	1.126	**2.480**	**2.746**	NA

*Values in bold indicate that there is significant difference between the two classifications based on a 95% confidence level. ASE: asymptotic standard error.

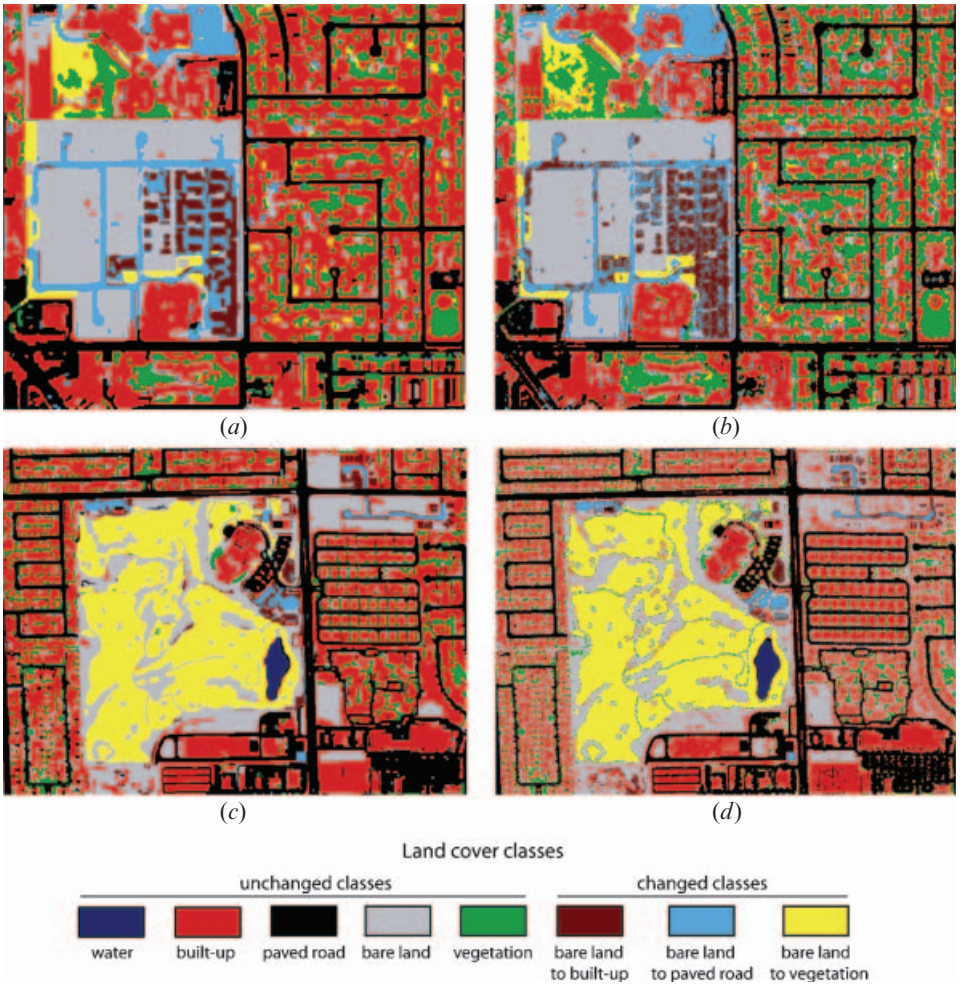

Figure 6. Four selected change detection results: (*a*) classification M1DTA; (*b*) classification M5DTA; (*c*) classification M2NNB; and (*d*) classification M5DTB.

Object-based change detection methods applied in the study revealed several advantages. First, the 'salt-and-pepper' noise can be reduced through object-based analysis. Second, object-based change detection is more efficient than per-pixel change detection in that the object-based approach generally deals with a considerably reduced number of units. For example, there were >1.8 million pixels in the imagery for *Site A* and 3.2 million pixels in the imagery for *Site B*. However, through the image segmentation process, the input data for *Site A* consisted of 6581 objects (i.e. 0.36% of the total number of pixels), and the input data for *Site B* consist of 11 570 objects (i.e. 0.35% of the total number of pixels). Thus, object-based analysis was more efficient in processing cost and time. In addition, objects can contain more information including shape properties and object relationships as well as spectral properties. This may make object-based image processing more powerful, although the additional information (e.g. shape properties) was not investigated in this research.

On the other hand, object-based change detection has several limitations which should be resolved in the future studies. Some researchers have conducted object-oriented change detection based on the post-classification comparison method, which results in problems cased by differences in objects geometry in the two dates of imagery under examination. This study removed these object (polygon) geometric problems by analysing the composite imagery, not each date of imagery. However, errors caused by the different look angles of the bi-temporal image datasets were still present in the composite imagery and accumulated through the subsequent analyses. Precise preprocessing (i.e. orthorectification) is necessary for the successful change detection in a high spatial domain with most change detection techniques including the methods investigated in the study. If both datasets were obtained by remote sensing systems with substantially different sensor positions, many errors would occur in feature (e.g. houses) boundaries, even after accurate geometric registration. The effect of shadows must be taken into consideration in urban areas that contain tall buildings and in areas with substantial local topographic relief.

5. Summary and conclusion

With the proliferation of high-spatial resolution satellite and aerial imagery in remote sensing, object-based image analysis techniques have provided many improvements and several advantages when compared with pixel-based image processing. In this study, we evaluated the object-based change detection methods based on correlation analysis and image segmentation techniques for two study sites with the bi-temporal QuickBird high-spatial resolution multispectral satellite imagery.

Both the *object correlation images* (OCIs) and *neighbourhood correlation images* (NCIs) yielded visually useful change information. For most land cover classes, there was no significant mean difference between object and neighbourhood variables (i.e. correlation, slope, and intercept) from the statistical *t*-test based on the reference data for *Site B*. Through the 16 change classification treatments, the following three aspects were examined in the study: (1) effectiveness of OCIs and/or NCIs in change classification, (2) comparison between two different classification algorithms applied (i.e. decision tree and nearest-neighbour), and (3) effectiveness of object-based change classification, compared with pixel-based analysis.

Incorporation of the OCIs or the NCIs into the object-based change classifications yielded higher accuracies regardless of the classification algorithm applied. Some of the change classifications incorporating the additional features were significantly more accurate than the change classifications without any additional features (e.g. M1DTA vs. M3DTA). However, there was no statistical difference between the change classification incorporating the OCIs and that incorporating the NCIs (i.e. Methods 1 and 2). This suggests that both contextual features generated from correlation analysis based on object and neighbourhood can provide valuable change information.

Two different classification algorithms were applied to the composite imagery. There was no significant difference between the classification results using each algorithm when the other conditions were held constant (e.g. M1DTA vs. M1NNA). One reason for this is that those classifications were conducted with the averaged brightness values per object, where complexity in spectral properties of the original imagery was much reduced. Consequently, the simple nearest-neighbour classifier

functioned as well as the machine-learning decision tree logic. Object-based change classification produced higher accuracies than per-pixel classification when the other conditions were held constant. However, the Kappa differences were not found to be significant at the 95% confidence level.

Most high-spatial resolution satellite imagery consists of four multispectral and one panchromatic bands, which are relatively small numbers of bands to produce successful change classification all the time. Thus, additional contextual features such as OCIs and NCIs can improve change classification accuracy. Future research should investigate the incorporation of multi-resolution image segmentation in object-based change detection and other change-detection application of these correlation analysis derivatives (e.g. fire-severity mapping).

Acknowledgements

This research was funded by the NASA REASoN project (NCC-1303008) titled 'Development of A Remote Sensing-assisted Decision Support System for Natural and Technological Hazards'. We are grateful to the Research and Development Imagery for Institutions (RADII) program by DigitalGlobe, Inc., for providing the QuickBird satellite remote sensing data.

References

BAATZ, M., BENZ, U., DEHGHANI, S. and HEYNEN, M., 2004, *eCognition User Guide 4* (Munich, Germany: Definiens Imagine GmbH).

BENZ, U., HOFMANN, P., WILLHAUCK, G., LINGENFELDER, I. and HEYNEN, M., 2004, Multi-resolution, object-oriented fuzzy analysis of remote sensing data for GIS-ready information. *ISPRS Journal of Photogrammetry and Remote Sensing*, **58**, pp. 239–258.

BLASCHKE, T., 2005, *A framework for change detection based on image objects*, In *Göttinger Geographische Abhandlungen*, S. Erasmi, B. Cyffka and M. Kappas (Eds), **113**, pp. 1–9, Göttingen. Available online at http://www.definieris.com/pdf/publications/GGRS2004_Blaschke_G001.pdf (accessed 11 January 2005).

BLASCHKE, T. and STROBL, J., 2001, What's wrong with pixels? Some recent developments interfacing remote sensing and GIS. In *Proceedings of GIS—Zeitschrift fur Geoinformationsysteme*, Heidelberg, pp. 12–17.

CONGALTON, R.G. and GREEN, K., 1999, *Assessing the Accuracy of Remotely Sensed Data: Principles and Practices* (New York: Lewis).

DEER, P., 1998, Digital change detection in remotely sensed imagery using fuzzy set theory. PhD Dissertation, University of Adelaide.

DEKOK, R., SCHNEIDER, T. and AMMER, U., 1999, Object based classification, applications in the alpine forest environment. *International Archives of Photogrammetry and Remote Sensing*, **32**, pp. 3–4.

FROHN, R.C., HINKEL, K.M. and EISNER, W.R., 2005, Satellite remote sensing classification of thaw lakes and drained thaw lake basins on the North Slope of Alaska. *Remote Sensing of Environment*, **97**, pp. 116–126.

GWET, K., 2002, *Computing Inter-Rater Reliability with the SAS System*, Series: Statistical Methods for Inter-Rater Reliability Assessment No. 3. Available online at: http://www.stataxis.com/files/articles/inter_rater_reliability_with_sas.pdf (accessed 24 January 2005).

HODGSON, M.E., JENSEN, J.R., TULLIS, J.A., RIORDAN, K.D. and ARCHER, C.M., 2003, Synergistic use of lidar and color aerial photography for mapping urban parcel imperviousness. *Photogrammetric Engineering and Remote Sensing*, **69**, pp. 973–980.

HUANG, X. and JENSEN, J.R., 1997, A machine-learning approach to automated knowledge-base building for remote sensing image analysis with GIS data. *Photgrammetric Engineering and Remote Sensing*, **63**, pp. 1185–1194.

IM, J. and JENSEN, J.R., 2005, A change detection model based on neighborhood correlation image analysis and decision tree classification. *Remote Sensing of Environment*, **99**, pp. 326–340.

IM, J., JENSEN, J.R. and TULLIS, J.A., 2005, Development of a remote sensing change detection system based on neighborhood correlation image analysis and intelligent knowledge-based systems. In *IEEE International Geoscience and Remote Sensing Symposium*, Seoul, Korea, 27 July, DVD-ROM.

JENSEN, J.R., 2005, *Introductory Digital Image Processing: A Remote Sensing Perspective 3rd* (Upper Saddle River, NJ: Prentice-Hall).

JENSEN, J.R., QUIJANO, M., HADLEY, B., IM, J., WANG, Z. and NEL, A.L., *et al.,* in press, Remote sensing agriculutural crop type for sustainable development in South Africa. *Geocarto International*, **21**, pp. 5–18.

LALIBERTE, A.S., RANGO, A., HAVSTAD, K.M., PARIS, J.F., BECK, R.F. and MCNEELY, R., *et al.,* 2004, Object-oriented image analysis for mapping shrub encroachment from 1937 to 2003 in southern New Mexico. *Remote Sensing of Environment*, **93**, pp. 198–210.

MUCHONEY, D., GOPAL, S., HODGES, J., MORROW, N., STRAHLER, A. and BORAK, J., *et al.,* 2000, Application of the MODIS global supervised classification model to vegetation and land cover mapping of central America. *International Journal of Remote Sensing*, **21**, pp. 1115–1138.

NIEMEYER, I., NUSSBAUM, S. and CANTY, M.J., 2005, Automation of change detection procedures for nuclear safeguards-related monitoring purposes. In *IEEE International Geoscience and Remote Sensing Symposium*, Seoul, Korea, 27 July, DVD-ROM.

QUINLAN, J.R., 2003, *Data Mining Tools See5 and C5.0*, St. Ives NSW, Australia: RuleQuest Research. Available online at: http://www.rulequest.com/see5-info.html (accessed 21 January 2005).

RULEQUEST RESEARCH, 2005, *C5.0 Release 2.01* (data mining software) (St. Ives, Australia: RuleQuest Research).

SOILLE, P., 2003, *Morphological Image Analysis: Principles and Applications*, 2nd ed (New York: Springer).

SYED, S., DARE, P. and JONES, S., 2005, Automatic classification of land cover features with high resolution imagery and lidar data: an object oriented approach. In *Proceedings of SSC2005 Spatial Intelligence, Innovation and Praxis: The National Biennial Conference of the Spatial Sciences Institute*, September.

TULLIS, J.A. and JENSEN, J.R., 2003, Expert system house detection in high spatial resolution imagery using size, shape, and context. *Geocarto International*, **18**, pp. 5–15.

WALTER, V., 2004, Object-based classification of remote sensing data for change detection. *ISPRS Journal of Photogrammetry and Remote Sensing*, **58**, pp. 225–238.